Integrin-linked kinase in muscle is necessary for the development of insulin resistance in diet-induced obese mice

Kang, Li; Mokshagundam, Shilpa; Reuter, Bradley; Lark, Daniel S.; Sneddon, Claire C.; Hennayake, Chandani

Published in:
Diabetes

DOI:
10.2337/db15-1434

Publication date:
2016

Document Version
Peer reviewed version

Integrin-linked kinase in muscle is necessary for the development of insulin resistance in diet-induced obese mice

Kang, Li; Mokshagundam, Shilpa; Reuter, Bradley; Lark, Daniel S.; Sneddon, Claire; Hennayake, Chandani; Williams, Ashley S.; Bracy, Deanna P.; James, Freyja D.; Pozzi, Ambra; Zent, Roy; Wasserman, David H.

Published in:
Diabetes

DOI:
10.2337/db15-1434

Publication date:
2016

Document Version
Peer reviewed version

Integrin-Linked Kinase in Muscle is Necessary for the Development of Insulin Resistance in Diet-Induced Obese Mice

Li Kang[1,2,3], Shilpa Mokshagundam[1], Bradley Reuter[1], Daniel S. Lark[1], Claire C. Sneddon[3], Chandani Hennayake[3], Ashley S. Williams[1], Deanna P. Bracy[1,2], Freyja D. James[1,2], Ambra Pozzi[1,4,5], Roy Zent[4,5], David H. Wasserman[1,2]

[1]Department of Molecular Physiology and Biophysics, Vanderbilt University, Nashville, TN, USA; [2]Mouse Metabolic Phenotyping Center, Vanderbilt University, Nashville, TN, USA; [3]Division of Molecular and Clinical Medicine, School of Medicine, University of Dundee, Dundee, UK; [4]Department of Medicine, Division of Nephrology, Vanderbilt University, Nashville, TN, USA; [5]Department of Medicine, Veterans Affairs Hospital, Nashville, TN, USA

Running title: Muscle ILK and insulin resistance

Address correspondence to: Li Kang, PhD, Division of Molecular and Clinical Medicine, School of Medicine, Level 5, Mailbox 12, University of Dundee, Dundee DD1 9SY, UK; Phone: +44 (0)1382 383019; Fax: +44 (0)1382 383598; E-mail: l.kang@dundee.ac.uk

The word count: 3691

Number of table and figures: 8

Abstract

Diet-induced muscle insulin resistance is associated with expansion of extracellular matrix (ECM) components such as collagens and the expression of collagen binding integrin, α2β1. Integrins transduce signals from ECM via their cytoplasmic domains, which bind to intracellular integrin binding proteins. The ILK-PINCH-parvin (IPP) complex interacts with the cytoplasmic domain of β integrin subunits and is critical for integrin signaling. In this study we defined the role of integrin-linked kinase (ILK), a key component of the IPP, in diet-induced muscle insulin resistance. Wildtype ($ILK^{lox/lox}$) and muscle-specific ILK-deficient ($ILK^{lox/lox}$HSA*cre*) mice were chow fed or high fat (HF) fed for 16wks. Body weight was not different between $ILK^{lox/lox}$ and $ILK^{lox/lox}$HSA*cre* mice. However, HF-fed $ILK^{lox/lox}$HSA*cre* mice had improved muscle insulin sensitivity relative to HF-fed $ILK^{lox/lox}$ mice as shown by increased rates of glucose infusion, glucose disappearance, and muscle glucose uptake during a hyperinsulinemic-euglycemic clamp. Improved muscle insulin action in the HF-fed $ILK^{lox/lox}$HSA*cre* mice was associated with increased insulin-stimulated phosphorylation of Akt and increased muscle capillarization. These results suggest that ILK expression in muscle is a critical component of diet-induced insulin resistance, which possibly acts by impairing insulin signaling and insulin perfusion through capillaries.

Introduction

Insulin resistance is a commonly associated risk factor for many pathophysiological conditions including diabetes, cardiovascular diseases, neurological changes, liver diseases, and sleep apnea (1,2). A defect in glucose utilization in the skeletal muscle is a major component of insulin resistance. The pathogenesis of muscle insulin resistance is not fully understood and pharmacological interventions that reduce insulin resistance are limited and often lose efficacy over time (e.g. biguanides) or have adverse side effects (e.g. thiazolidinediones) (3). Our recent studies have suggested a novel role for extramyocellular factors in regulating muscle insulin action. Expansion of extracellular matrix (ECM) components such as the collagens and the expression of the collagen binding integrin α2β1 are associated with high fat (HF) diet-induced muscle insulin resistance (4). The ECM is in direct contact with the muscle capillaries. Defects in recruitment of muscle capillaries contribute to the development of muscle insulin resistance (5). Transduction of ECM signals through integrins requires interaction of the integrin cytoplasmic domains with cellular proteins. To investigate the link between ECM-integrin signaling and muscle insulin resistance, we studied a highly-conserved central downstream component of the ECM-integrin signaling, integrin-linked kinase (ILK) and its role in muscle insulin resistance.

ILK is a pseudo-kinase with adaptor function. It is a central component of the ILK-PINCH-parvin complex (IPP) (6). This complex binds to the cytoplasmic domain of β integrin subunits. The IPP complex functions as an adaptor between integrins and the actin cytoskeleton, therefore regulating multiple cellular functions including cell spreading, migration, proliferation, survival, and cell-cell adhesion (7,8). IPP also acts as a hub of the downstream of integrin signaling that regulates several other signaling pathways. The IPP complex associates with the

receptor tyrosine kinase (RTK) pathways (e.g. insulin receptor pathway) through protein NCK2, which binds to PINCH (9). Considering the important role of RTK signaling in metabolism, we propose that ILK is fundamental to metabolic regulation. In the current study, we tested the hypothesis that the expansion of ECM collagen will amplify activation of integrin receptor signaling through ILK and regulate insulin signaling, thereby contributing to muscle insulin resistance. Muscle-specific ILK knockout mice were utilized to investigate the contribution of ILK signaling in chow-fed and HF-fed mice, a well-established model of insulin resistance (10). Our results reveal that integrin receptor signaling through ILK is critical to the pathogenesis of insulin resistance.

Research Design and Methods

Mouse Models

All mice were housed in cages under conditions of controlled temperature and humidity with a 12-h light/dark cycle. Transgenic mice expressing *Cre* under a human alpha-skeletal actin (HSA or *ACTA1*) promoter (Jackson Laboratory Stock# 006149) were crossed with floxed ILK mice ($ILK^{lox/lox}$) (11,12), to obtain the muscle-specific ILK deficient mice ($ILK^{lox/lox}$HSA*cre*). All mice were on a C57BL/6J background and were fed either a chow (LabDiet #5001), or HF diet (BioServ F3282) starting at 3 weeks of age (at weaning), for 16 weeks unless stated otherwise. All mice had ad libitum access to food and water. The calorie breakdown was 29% protein, 13% fat, and 58% carbohydrate for the chow diet, and 15% protein, 59% fat, and 26% carbohydrate for the HF diet. Noticeably, the HF diet is also a low protein, low carbohydrate diet compared to the chow diet. Male mice were used in the study because of their more robust insulin-resistant phenotype after HF feeding as compared to female mice. In addition, female mice introduce a number of biological variables for which there is currently limited data and as such it is difficult to adequately interpret results. Body composition was determined by a mq10 nuclear magnetic resonance analyzer (Brucker optics). The Vanderbilt and Dundee Animal Care and Use Committee approved all animal procedures.

Hyperinsulinemic-Euglycemic Clamp (IC_v)

Catheters were implanted in a carotid artery and a jugular vein of mice for sampling and intravenous infusions 5 days before IC_v (13). IC_v (4mU/kg/min) was performed on 5hr-fasted mice since they have ample glycogen stores and do not undergo the dramatic weight loss seen after an overnight fast (13). [3-^{3}H]glucose was infused to determine glucose flux rates (14).

Blood glucose was clamped at ~150mg/dL using a variable glucose infusion (GIR). Mice received washed erythrocytes from donors to prevent the drop in hematocrit that would otherwise occur. IC_v was achieved by assessment of blood glucose every 10min with GIR adjusted as needed. Blood was taken at 80-120min for the determination of [3-^{3}H]glucose. Clamp insulin was determined at t=100 and 120min. At 120min the clamp was sustained and a 13μCi 2[^{14}C]deoxyglucose ([^{14}C]2DG) bolus was administered. Blood was taken at 122-155min for [^{14}C]2DG determination. After the last sample, mice were anesthetized and tissues were excised.

IC_v Plasma and Tissue Sample Processing and Glucose Flux Rate Determination

Plasma insulin was determined using the insulin ELISA kit (Millipore). Non-esterified fatty acid (NEFA) concentrations were measured by an enzymatic colorimetric assay (NEFA C kit, Wako Chemicals). Liver triglyceride was measured using the GPO triglyceride kit (Pointe Scientific, Cat#T7532) in ~100mg frozen liver. Plasma and tissue radioactivity of [3-^{3}H]glucose, [^{14}C]2DG, and [^{14}C]2DG-6-phosphate were determined as described (15). Glucose appearance (Ra), endogenous glucose appearance (EndoRa), and glucose disappearance (Rd) rates were determined using non-steady-state equations (16). The glucose metabolic index (Rg) was calculated as described (17).

Immunohistochemistry

ILK, collagen IV (ColIV), laminin, CD31, and Von Willebrand Factor (vWF) were assessed by immunohistochemistry in paraffin-embedded gastrocnemius tissue sections (5μm) using the following primary antibodies: anti-ILK (1:150, Santa Cruz, sc-20019), anti-ColIV

(1:100; Abcam, ab6586), anti-laminin (1:3000, DakoCytomation, Z0097), anti-CD31 (1:200, BD Biosciences, 550274), and anti-vWF (1:3000, DakoCytomation, A0082). Slides were lightly counterstained with Mayer's hematoxylin. The EnVision+HRP/DAB System (DakoCytomation) was used to produce localized, visible staining. Images were captured using a Q-Imaging Micropublisher camera mounted on an Olympus upright microscope. Immunostaining was quantified by ImageJ or BIOQUANT Life Science 2009. ILK, ColIV, and laminin protein was measured by the integrated intensity of staining. Muscle vascularity was determined by counting CD31 positive structures and by measuring areas of vWF positive structures. Average fiber diameter of gastrocnemius muscle was manually measured from laminin staining images. At least 15 fibers were measured per image and 6 images were measured per animal.

Immunoprecipitation and Immunoblotting

Gastrocnemius was homogenized as described (4). Protein (40μg) was applied to SDS-PAGE gel. The following antibodies were used to detect respective proteins: ILK (1:1000, Santa Cruz, sc-20019), insulin receptor substrate 1 (IRS-1) (1:1000, Cell Signaling, #2382), phospho-Akt (Ser473) (1:1000, Cell Signaling, #9271), total Akt (1:1000, Cell Signaling, #9272), phospho-P38 (1:1000, Cell Signaling, #9211), total P38 (1:1000, Cell Signaling, #9212), phospho-ERK1/2 (1:2000, Cell Signaling, #4370), total ERK1/2 (1:1000, Cell Signaling, #4695), phospho-JNK (1:1000, Cell Signaling, #9251) and total JNK (1:1000, Cell Signaling, #9252), and p-Tyr (PY99) (1:1500, Santa Cruz, sc-7020). GAPDH (1:2000, Cell Signaling, #5174) was used as a loading control. For immunoprecipitation, 500μg of protein was pre-cleared with 50μL of protein A/G PLUS-Agarose beads by incubation at 4°C for 1 hour. Protein supernatant was then incubated with the insulin receptor β (IRβ) antibody (1:50, Cell Signaling, #3025) at 4°C for

overnight. Then, 20µL protein A/G PLUS-Agarose was added and incubated. The mixture was centrifuged and the supernatant removed. The beads were washed four times and centrifugation was repeated. Beads were re-suspended and applied to SDS-PAGE gel. Immunoblots were probed with primary antibodies for p-Tyr (PY99) (1:1500, Santa Cruz, sc-7020) and IRβ (4B8) (1:1000, Cell Signaling, #3025).

Food Intake and Wet Gastrocnemius Weight

Food intake and gastrocnemius muscle weight were measured in HF-fed mice after 27 weeks of HF feeding. Average food intake for light and dark cycle was measured by Promethion System (Sable Systems International). Wet gastrocnemius muscle was collected and weighed from 5h-fasted mice.

Statistical Analysis

Data are expressed as mean ± SEM. Statistical analyses were performed using either student's t test or two-way ANOVA followed by Tukey's post hoc tests as appropriate. The significance level was at $p<0.05$.

Results

To elucidate the role of ILK in muscle insulin resistance, muscle-specific ILK deficient mice ($ILK^{lox/lox}$HSA*cre*) and their wild type littermate controls ($ILK^{lox/lox}$) were fed a chow or a HF diet, which has been previously defined to induce muscle insulin resistance (10). Immunohistochemical staining of ILK revealed that ILK was exclusively deleted from the muscle fibers of $ILK^{lox/lox}$HSA*cre* mice, but remained in the other cell types, such as endothelial cells (Figure 1A). HF diet feeding alone did not affect ILK expression in the muscle (Figure 1B). Deletion of ILK in skeletal muscle fibers did not affect weight gain of mice on either diet (Figure 2A). The percent fat and lean masses did not differ between $ILK^{lox/lox}$ and $ILK^{lox/lox}$HSA*cre* mice regardless of diet (Figures 2B and 2C). Consistent with unchanged percent lean mass, wet gastrocnemius muscle weight was not different between HF-fed $ILK^{lox/lox}$ and $ILK^{lox/lox}$HSA*cre* mice (Figure 2D). Food intake was the same between the two groups of mice on HF diet (Figure 2E).

To investigate the metabolic consequences of muscle-specific deletion of ILK, mice underwent ICv clamps. Basal arterial glucose (t=0min) was not different between chow-fed $ILK^{lox/lox}$ and $ILK^{lox/lox}$HSA*cre* mice, but was significantly decreased in the HF-fed $ILK^{lox/lox}$HSA*cre* mice (Figures 3A and 3B). IC_v glucose during the steady state of the clamp (t=80-120min) was 150mg/dL in both genotypes and in mice on both diets (Figures 3A and 3B). In chow-fed mice, ICv GIR was the same between $ILK^{lox/lox}$ and $ILK^{lox/lox}$HSA*cre* mice, indicating no difference in insulin sensitivity (Figure 3C). Basal EndoRa and Rd were the same between chow-fed $ILK^{lox/lox}$ and $ILK^{lox/lox}$HSA*cre* mice (Figure 3E). EndoRa was equivalently suppressed and Rd was equivalently increased during the ICv in both genotypes (Figure 3E). In contrast, ICv GIR was markedly increased in the HF-fed $ILK^{lox/lox}$HSA*cre* mice compared to HF-

fed ILK$^{lox/lox}$ mice, indicating an improved response to insulin (Figure 3D). This increase in GIR in ILK$^{lox/lox}$HSA*cre* was due to an increase in clamp Rd (Figure 3F). The inhibition of EndoRa during the ICv was unaffected by genotypes, emphasizing the muscle-specific effect on insulin action (Figure 3F). Increased clamp Rd in HF-fed ILK$^{lox/lox}$HSA*cre* mice was attributed to both increased glycolytic and glucose storage rates, which were estimated by the rate of plasma ^{3}H-H_2O accumulation during the ICv clamp (Figure S1).

Rg in muscles was decreased in HF-fed ILK$^{lox/lox}$ mice compared to chow-fed ILK$^{lox/lox}$ mice, indicative of HF diet-induced insulin resistance (Figure 4A). Muscle Rg was unaffected by ILK deletion in chow-fed mice. Remarkably, the HF-induced muscle Rg impairment was absent in the HF-fed ILK$^{lox/lox}$HSA*cre* mice (Figure 4A). Rg in adipose tissue was not different between ILK$^{lox/lox}$ and ILK$^{lox/lox}$HSA*cre* mice regardless of diet (Figure 4A). Taken together, these data suggest that muscle-specific deletion of ILK in mice improved HF diet-induced insulin resistance specifically in muscle. This improvement of insulin resistance is independent of adiposity.

Basal plasma NEFA concentrations were not affected by genotype or diet (Figure 4B). Despite the same plasma NEFA concentrations between chow-fed ILK$^{lox/lox}$ and ILK$^{lox/lox}$HSA*cre* mice during the ICv, ICv plasma NEFA was significantly lower in the HF-fed ILK$^{lox/lox}$HSA*cre* mice compared to HF-fed ILK$^{lox/lox}$ mice, indicative of an improved ability of insulin to inhibit lipolysis (Figure 4B). While basal arterial insulin was not affected by ILK deletion in the chow-fed mice, muscle-specific ILK deletion significantly lowered basal arterial insulin in the HF-fed mice, suggesting improved insulin sensitivity (Figure 4C). It is worth noting that basal arterial insulin concentration in HF-fed ILK$^{lox/lox}$HSA*cre* mice was still substantially higher than that in chow-fed mice. These data together with a defect seen in

glycogen storage in HF-fed ILK$^{lox/lox}$HSA*cre* mice compared to that in chow-fed mice (Figure S1) suggest that HF-fed ILK$^{lox/lox}$HSA*cre* mice were still insulin resistant despite the marked improvement in muscle Rg. Insulin concentrations during the ICv were equivalent between genotypes (Figure 4C). Even though insulin action in the liver as assessed by EndoRa was unaffected (Figure 3F), liver triglyceride content was significantly decreased in the HF-fed ILK$^{lox/lox}$HSA*cre* mice compared to HF-fed ILK$^{lox/lox}$ mice (Figure 4D). This suggests that the muscle metabolic status can convey a signal to liver that reduces triglyceride accumulation. Similarly, we also found changes in the status of adipose inflammation (Figure S2). Gene expression of total macrophage marker F4/80 was increased in ILK$^{lox/lox}$HSA*cre* mice compared to ILK$^{lox/lox}$ mice regardless of diet (Figure S2A). Gene expression of the pro-inflammatory marker TNFα was increased in ILK$^{lox/lox}$ mice by HF feeding, but interestingly this diet effect was absent in ILK$^{lox/lox}$HSA*cre* mice (Figure S2B). In contrast, gene expression of the anti-inflammatory markers IL-10 and Arg-1 was increased in HF-fed ILK$^{lox/lox}$HSA*cre* mice compared to HF-fed ILK$^{lox/lox}$ mice (Figure S2C). These effects of muscle ILK deletion on liver and adipose tissue were associated with an increase in IL-6 mRNA levels in muscle of HF-fed ILK$^{lox/lox}$HSA*cre* mice compared to HF-fed ILK$^{lox/lox}$ mice (Figure S2D).

We further investigated the mechanisms by which HF-fed ILK$^{lox/lox}$HSA*cre* mice had improved muscle insulin resistance. Elevated ECM deposition has been associated with HF diet-induced muscle insulin resistance (4,18,19). We examined the ECM collagen and laminin content in the muscle. Consistent with previous findings (4), muscle collagen IV deposition was increased by 2-fold with HF feeding in ILK$^{lox/lox}$ mice, while muscle laminin deposition was not affected (Figures 5A and 5B). Neither collagen IV nor laminin was affected by ILK deletion. Moreover, the average fiber diameter of gastrocnemius muscle was not changed by genotype or

HF diet (Figure 5C). Interestingly, improved muscle insulin resistance in HF-fed ILK$^{lox/lox}$HSA*cre* mice was associated with increased CD31 staining in muscle of HF-fed ILK$^{lox/lox}$HSA*cre* mice compared to HF-fed ILK$^{lox/lox}$ mice, indicating increased CD31-positive capillarization (Figures 5D and 5E). There was no change in vWF staining indicating that larger vessels were unaffected (Figures 5D and 5E).

We next investigated insulin signaling in the muscle. While improved muscle insulin resistance in HF-fed ILK$^{lox/lox}$HSA*cre* mice was not associated with increased phosphorylation of insulin receptor (Figures 6A and 6B) or insulin receptor substrate-1 (IRS-1) (Figures 6C and 6D), improved muscle insulin action was associated with increased phosphorylated and total Akt/PKB (Figures 6C and 6E). This effect is specific to insulin-stimulated conditions as phosphorylated and total Akt/PKB was not increased in the basal 5h-fasted muscles (Figures 6F and 6G).

Mitogen-activated protein kinases (MAPKs) have been shown to negatively regulate endothelial cell survival, proliferation, and differentiation (20). We investigated whether the increased muscle capillarization in the HF-fed ILK$^{lox/lox}$HSA*cre* mice were associated with altered MAPKs pathway. While HF diet feeding caused an increase in ratios of p-P38/P38 and p-JNK/JNK, this diet effect was absent in the HF-fed ILK$^{lox/lox}$HSA*cre* mice (Figures 7A-D). Moreover, p-ERK/ERK ratio was decreased in the HF-fed ILK$^{lox/lox}$HSA*cre* compared to HF-fed ILK$^{lox/lox}$ mice (Figures 7E and 7F). These results are consistent with the prior assertion that capillarization may be upregulated by a decrease in MAPK activation (20).

Discussion

ECM expansion and the interaction of protein constituents with the cell surface receptor integrin α2β1 have been found recently to contribute to the pathogenesis of HF diet-induced muscle insulin resistance (4,18,19). There appear to be α subunit specific effects of integrin-ligand binding (21), as integrin α1β1 does not appear to contribute to diet-induced muscle insulin resistance (4,22). The ILK pseudokinase, is a central component of the IPP complex which binds to the cytoplasmic domains of both integrin α1β1 and α2β1, and therefore its expression may be a better reflection of the integrated integrin response. Here we show that while muscle-specific deletion of ILK has no effect in lean, chow-fed mice it, improves HF diet-induced muscle insulin resistance. The improvement in insulin-stimulated glucose fluxes is specific to muscle as the ability of insulin to inhibit hepatic glucose production and to stimulate glucose uptake in adipose tissue are not affected. We further discovered that improved muscle insulin resistance in the ILK-deficient mice is associated with increased phosphorylation of Akt and increased muscle capillarization. These findings show that ILK is central to insulin resistance associated with HF feeding. An extension of these findings is that ILK inhibition is of potential therapeutic use in the treatment of diabetes and other insulin resistance-associated metabolic disorders.

We establish a working model in the current study by which insulin signaling and integrin signaling interact at the level of Akt (Figure 8). Although ILK is a pseudokinase, it contains a catalytically inactive remnant of an active kinase that uses its substrate recognition motif to interact with other proteins that have well-conserved motifs required for eukaryotic protein kinase activity (23). Our results show that muscle-specific deletion of ILK increases phosphorylation of Akt at Ser 473 in HF-fed mice and this effect is specific to insulin stimulation

as basal Akt phosphorylation was not affected in these mice. While the precise steps how ILK regulates phosphorylation of Akt during the stimulation of insulin are uncertain, studies of ILK in cell adhesion and survival provide a basis for linkage. Rictor directly interacts with ILK and regulates Akt phosphorylation promoting cancer cell survival (24). Moreover, it is widely proposed that ILK associates with the receptor tyrosine kinase (RTK) pathways (e.g. insulin receptor pathway) through protein NCK2, which binds to PINCH, one of the components of the IPP complex (9). The other possibility is that ILK controls Akt activity by regulating its subcellular localization as ILK-binding partners, α- and β-parvins induce the recruitment of Akt to the plasma membrane (25,26). It is noteworthy that the majority of studies in ILK has focused on signaling involved in cell spreading, adhesion, migration and survival, therefore the ILK-mediated signaling in metabolic regulation could be significantly different.

Reduction in blood flow to the muscle correlates with insulin resistance and the number of capillaries that perfuse the muscle is positively related to peripheral insulin action (27). In the current study, we found that improvement of muscle insulin resistance in HF-fed obese mice by muscle-specific ILK deletion is associated with increased expression of vascular/endothelial marker, CD31 in muscle. This finding is consistent with a previous study that shows that genetic integrin α2β1 deletion-improved muscle insulin resistance is associated with increased muscle capillaries (4). In contrast, exacerbated insulin resistance in HF-fed matrix metalloproteinase 9 (MMP9)-deficient mice, where muscle collagen deposition is increased, is associated with decreased muscle capillaries (19). Activation of MAPK pathways negatively regulate endothelial cell survival, proliferation, and differentiation (20). We found that increased muscle capillarization in the HF-fed ILK deficient mice are associated with decreased phosphorylation of several MAPKs including P38, ERK1/2, and JNK. The regulation of ILK in the MAPK

pathways is thought to be through Ras suppression protein 1 (RSU1), which binds to ILK via Pinch-1 (28). Taken together, these results indicate that ILK expression in muscle may stimulate activation of various MAPKs pathways, which in turn inhibit capillary proliferation and endothelial function (Figure 8). Both inhibited phosphorylation of Akt and inhibited capillary proliferation induced by muscle ILK expression during insulin stimulation are likely mechanisms that contribute to the development of insulin resistance in the presence of HF diet (Figure 8).

The effect of muscle-specific deletion of ILK on overall total blood flow in muscle is unknown. It is unlikely that ILK deletion has a major impact on muscle blood flow as the expression of vWF, a vascular marker for bigger vessels was not changed in the ILK deficient mice (Figures 5D and 5E). However, the increase in CD31 suggests that capillarization is increased. We hypothesize that improved muscle capillarization leads to greater exchange of insulin and other hormones from blood to muscle. Improved insulin access to muscle could contribute to improved insulin action in the HF-fed ILK deficient mice.

It is worth noting that considerable evidence in the literature suggests that HF diet-induced insulin resistance in skeletal muscle is associated with a remodeling of actin cytoskeleton (29). ILK, as a central component of the IPP complex which links integrins to actin cytoskeleton is essential for actin cytoskeleton organization and morphology (30). It is possible that deletion of ILK in muscle improves HF diet-induced insulin resistance through effects on reorganization of actin cytoskeleton. Moreover, it is possible that deletion of ILK in muscle may cause an alteration in muscle fiber type during HF feeding. This seems unlikely since Gheyara et al. has previously shown that ILK deletion does not change muscle fiber type proportions or distribution in the quadriceps of chow-fed mice (31). Nevertheless, we cannot rule out that a

switch in muscle fiber type to a more oxidative profile could occur during HF feeding and contribute to improved muscle insulin resistance in mice lacking muscle ILK.

It has been previously shown that muscle-specific deletion of ILK causes a progressive muscular dystrophy (31). This phenomenon is associated with disrupted focal adhesion proteins, including vinculin, paxillin, focal adhesion kinase, dystrophin, and the integrin α7β1 specifically at the myofascial junction regions. Gheyara et al. reported that the muscle damage was limited to the myofascial junction regions in young ILK mutant mice (31). Our current study focused at the muscle fiber level and was able to show that ILK was specifically deleted from the muscle fibers using immunohistochemistry. We showed that muscle collagens and laminin expression were not affected by ILK deletion. Importantly, we showed that total body weight and the %fat and %lean mass of both chow-fed and HF-fed mice were unchanged by ILK deletion. These results suggest that while ILK deletion may have aging-related structure and focal adhesion phenotypes in the myofascial junction areas, it retains a robust insulin-stimulatory response.

The development of pharmacological inhibition of ILK by small-molecule inhibitors has primarily focused on inhibiting its kinase activity (32,33). Because ILK is a scaffold protein rather than a kinase, none of these inhibitors are specific to ILK. Therefore, we believe that the development of pharmacological inhibition of ILK that targets its binding motifs is under high demand in future studies. Our studies show that ILK deletion has a remarkable impact on improving insulin sensitivity. Thus, these studies further implicate the importance of inhibition of ILK in the setting of diabetes and associated metabolic disorders.

In conclusion, our results suggest that muscle-specific deletion of ILK markedly improves muscle insulin sensitivity in HF-fed insulin resistant mice via increased phosphorylation of Akt in addition to increased muscle capillarization. The increased

capillarization is associated with decreased phosphorylation of MAPKs. These studies are the first linking ECM-integrin signaling to muscle insulin resistance via ILK and provide a mechanistic framework for the importance of ECM-integrin-ILK in metabolic regulation. The results open the door to the development of inhibitors of ILK signaling in the treatment of insulin resistance and its related metabolic disorders.

Acknowledgements

This work was supported by National Institutes of Health Grants DK054902 (D.H.W.) and DK059637 (Vanderbilt Mouse Metabolic Phenotyping Center), and was in part supported by VA Merit Review 1I01BX002196 (R.Z.) and 1I01BX002025 (A.P.), National Institutes of Health Grants RO1-DK083187 (R.Z.), RO1-DK075594 (R.Z.), RO1-DK066921 (R.Z.), RO1-CA162433 (A.P.), RO1-DK095761 (A.P.) and T32-DK070061 (D.S.L.). L.K. is supported by European Commission Marie Curie International Incoming Fellowship (FP7-PEOPLE-2013-IIF) and TENOVUS Scotland. The ILK floxed mice were generously provided by Professor Reinhard Fässler of Max Planck Institute of Biochemistry in Martinsried, Germany. Dr. Li Kang, University of Dundee, is the guarantor of this work and, as such, had full access to all the data in the study and takes responsibility for the integrity of the data and the accuracy of the data analysis. The authors receive no editorial assistance.

Author Contributions

L.K., experimental design, researched data, contributed discussion, and wrote manuscript; S.M., B.R., D.S.L., C.C.S., C.H., D.P.B., F.D.J. researched data and reviewed/edited manuscript; A.S.W., contributed discussion, and reviewed/edited manuscript; A.P., R.Z., and D.H.W., experimental design, reviewed data, contributed discussion, and reviewed/edited manuscript. All authors approved the final version of this manuscript.

Duality of Interest

The authors declare that there is no duality of interest associated with this manuscript.

Figure Legends

Figure 1. Protein expression of ILK in muscle. (A) Immunohistochemical staining of ILK in paraffin-embedded gastrocnemius sections from chow-fed mice (n=5). The magnification of images was 20X. Representative images are presented. Arrow heads indicate intact ILK expression in non-myocytes. (B) Western Blotting of ILK in whole gastrocnemius muscle lysates from chow-fed and HF-fed $ILK^{lox/lox}$ mice (n=3-4). All data are represented as mean ± SEM. Data are normalized to Chow $ILK^{lox/lox}$. HF, high fat.

Figure 2. Body weight, body composition, gastrocnemius weight, and food intake of the muscle-specific ILK deficient mice. (A) Body weights of chow-fed and HF-fed $ILK^{lox/lox}$ and $ILK^{lox/lox}$HSA*cre* mice up to 14 weeks of diet starting at 3 weeks of age (n=4-12). (B-C) Percent fat and lean masses were determined in mice after 14 weeks of diet (n=4-12). (D) Gastrocnemius muscle was collected and weighed in 5hr-fasted mice after 27 weeks of HF diet (n=5). (E) Food intake during the light and dark cycle was measured in mice after 27 weeks of HF diet (n=4). All data are represented as mean ± SEM. HF, high fat.

Figure 3. Insulin action as assessed by the hyperinsulinemic-euglycemic clamp (ICv). Mice underwent ICv experiments after 16 weeks of HF or chow diet feeding at 19 weeks of age. (A-B) Blood glucose during the ICv (n=5-9). (C-D) Glucose infusion rate during the ICv (n=5-9). (E-F) Endogenous glucose appearance (EndoRa) and glucose disappearance (Rd) rates were determined by [3-^{3}H]glucose (n=5-9). All data are represented as mean ± SEM. *p<0.05 HF-fed $ILK^{lox/lox}$ vs. HF-fed $ILK^{lox/lox}$HSA*cre*. $^{\#}p$<0.05 Basal vs. Clamp with the same genotype. *§*, p<0.05 for the main genotype effect. HF, high fat.

Figure 4. Muscle glucose uptake, circulating insulin, plasma non-esterified fatty acid (NEFA), and liver triglyceride. (A) Rg, an index of glucose metabolic rate was determined by 2-[^{14}C]deoxyglucose (n=5-9). (B) Plasma NEFA was determined at basal (-15 and -5min) and during the steady state of the ICv (80 and 120min) (n=5-9). (C) Plasma insulin concentration was measured at basal (-15 and -5min) and during the steady state of the ICv (100 and 120min) (n=5-9). (D) Liver triglyceride was determined in liver samples collected at the end of the ICv (n=5-9). All data are represented as mean ± SEM. $^{\#}p<0.05$ Chow vs. HF with the same genotype. $*p<0.05$. HF, high fat. SVL, superficial vastus lateralis.

Figure 5. Muscle ECM deposition, fiber diameter and vascular markers of the muscle-specific ILK deficient mice. (A) Immunohistochemical detection of collagen IV and laminin in paraffin-embedded gastrocnemius sections (n=5-9). The magnification of images was 20X. Representative images are presented. (B) Values represent mean ± SEM of integrated intensity of staining for collagen IV and laminin. Data are normalized to Chow ILK$^{lox/lox}$. (C) Average fiber diameter was manually measured from laminin staining images (n=5-9). (D) Immunohistochemical staining of CD31 and vWF in paraffin-embedded gastrocnemius sections (n=5-9). The magnification of images was 20X. Representative images are presented. (E) Values represent mean ± SEM of numbers of CD31 positive structures, or of areas occupied by vWF positive structures. Data are normalized to Chow ILK$^{lox/lox}$. * and $^{\#}$ indicate $p<0.05$. HF, high fat. vWF, Von Willebrand Factor.

Figure 6. Insulin signaling in the muscle. Muscle homogenates were prepared from gastrocnemius collected from mice post the hyperinsulinemic-euglycemic clamp *(A-E)* or from mice after a basal 5h fast *(F-G)*. (A) IRβ was immunoprecipitated followed by immunoblotting of pY99 and IRβ. Representative bands are presented (n=4-6). (B) Quantitative data for Panel *(A)*. (C) Phosphorylation of IRS-1 was determined by immunoblotting of pY99 at 180kDa. Total IRS-1, p-Akt, and total Akt was measured by Western blotting. Representative bands are presented (n=4-6). (D) Quantitative date for the Western blotting of PY99 at 180kDa and total IRS-1 from Panel *(C)*. (E) Quantitative data for the Western blotting of phosphorylated Akt and total Akt from Panel *(C)*. Data are normalized to Chow $ILK^{lox/lox}$. (F) Western blotting of phosphorylated Akt and total Akt in basal 5h-fasted gastrocnemius tissues (n=4). (G) Quantitative data for Panel *(F)*. All data are represented as mean ± SEM. $^{\#}p<0.05$ Chow vs. HF with the same genotype. $^{*}p<0.05$. HF, high fat. IRβ, insulin receptor β. IRS-1, insulin receptor substrate 1. pY, phospho-tyrosine.

Figure 7. P38, JNK, and ERK mitogen-activated protein kinases in the muscle. Western blotting of phosphorylated P38 and total P38 *(A)*, phosphorylated JNK and total JNK *(C)*, and phosphorylated ERK and total ERK *(E)* in gastrocnemius homogenates isolated from mice post the hyperinsulinemic-euglycemic clamp. Representative bands are presented (n=4-6). (B, D, and F) Quantitative data for the Western blotting. All data are represented as mean ± SEM. Data are normalized to Chow $ILK^{lox/lox}$. $^{\#}p<0.05$ Chow vs. HF with the same genotype. $^{*}p<0.05$. HF, high fat.

Figure 8. Proposed mechanisms by which ECM-integrin-ILK signaling regulates muscle insulin resistance in HF-fed mice. It is proposed that ILK will inhibit phosphorylation of Akt in the presence of insulin stimulation. ILK also stimulates the phosphorylation and activation of JNK, P38, and ERK1/2 mitogen-activated protein kinases, which in turn inhibits capillary proliferation and therefore endothelial function in the muscle. Both decreased phosphorylation of Akt and inhibited capillary proliferation contribute to muscle insulin resistance during the HF feeding. HF, high fat. MAPKs, mitogen-activated protein kinases. (-) Represents diminished effects. (+) Represents potentiated effects.

References

1. Dineley KT, Jahrling JB, Denner L. Insulin resistance in Alzheimer's disease. *Neurobiology of disease.* 2014;72 Pt A:92-103.

2. Reutrakul S, Van Cauter E. Interactions between sleep, circadian function, and glucose metabolism: implications for risk and severity of diabetes. *Annals of the New York Academy of Sciences.* 2014;1311:151-173.

3. Inzucchi SE, Bergenstal RM, Buse JB, Diamant M, Ferrannini E, Nauck M, Peters AL, Tsapas A, Wender R, Matthews DR. Management of hyperglycaemia in type 2 diabetes: a patient-centered approach. Position statement of the American Diabetes Association (ADA) and the European Association for the Study of Diabetes (EASD). *Diabetologia.* 2012;55(6):1577-1596.

4. Kang L, Ayala JE, Lee-Young RS, Zhang Z, James FD, Neufer PD, Pozzi A, Zutter MM, Wasserman DH. Diet-induced muscle insulin resistance is associated with extracellular matrix remodeling and interaction with integrin alpha2beta1 in mice. *Diabetes.* 2011;60(2):416-426.

5. Bonner JS, Lantier L, Hocking KM, Kang L, Owolabi M, James FD, Bracy DP, Brophy CM, Wasserman DH. Relaxin treatment reverses insulin resistance in mice fed a high-fat diet. *Diabetes.* 2013;62(9):3251-3260.

6. Legate KR, Montanez E, Kudlacek O, Fassler R. ILK, PINCH and parvin: the tIPP of integrin signalling. *Nature reviews Molecular cell biology.* 2006;7(1):20-31.

7. Hannigan G, Troussard AA, Dedhar S. Integrin-linked kinase: a cancer therapeutic target unique among its ILK. *Nature reviews Cancer.* 2005;5(1):51-63.

8. Elad N, Volberg T, Patla I, Hirschfeld-Warneken V, Grashoff C, Spatz JP, Fassler R, Geiger B, Medalia O. The role of integrin-linked kinase in the molecular architecture of focal adhesions. *Journal of cell science.* 2013;126(Pt 18):4099-4107.

9. McDonald PC, Fielding AB, Dedhar S. Integrin-linked kinase--essential roles in physiology and cancer biology. *Journal of cell science.* 2008;121(Pt 19):3121-3132.

10. Surwit RS, Kuhn CM, Cochrane C, McCubbin JA, Feinglos MN. Diet-induced type II diabetes in C57BL/6J mice. *Diabetes.* 1988;37(9):1163-1167.

11. Grashoff C, Aszodi A, Sakai T, Hunziker EB, Fassler R. Integrin-linked kinase regulates chondrocyte shape and proliferation. *EMBO reports.* 2003;4(4):432-438.

12. Sakai T, Li S, Docheva D, Grashoff C, Sakai K, Kostka G, Braun A, Pfeifer A, Yurchenco PD, Fassler R. Integrin-linked kinase (ILK) is required for polarizing the epiblast, cell adhesion, and controlling actin accumulation. *Genes & development.* 2003;17(7):926-940.

13. Ayala JE, Bracy DP, McGuinness OP, Wasserman DH. Considerations in the design of hyperinsulinemic-euglycemic clamps in the conscious mouse. *Diabetes.* 2006;55(2):390-397.

14. Berglund ED, Li CY, Poffenberger G, Ayala JE, Fueger PT, Willis SE, Jewell MM, Powers AC, Wasserman DH. Glucose metabolism in vivo in four commonly used inbred mouse strains. *Diabetes.* 2008;57(7):1790-1799.

15. Ayala JE, Bracy DP, Julien BM, Rottman JN, Fueger PT, Wasserman DH. Chronic treatment with sildenafil improves energy balance and insulin action in high fat-fed conscious mice. *Diabetes.* 2007;56(4):1025-1033.

16. Steele R, Wall JS, De Bodo RC, Altszuler N. Measurement of size and turnover rate of body glucose pool by the isotope dilution method. *Am J Physiol.* 1956;187(1):15-24.
17. Kraegen EW, James DE, Jenkins AB, Chisholm DJ. Dose-response curves for in vivo insulin sensitivity in individual tissues in rats. *Am J Physiol.* 1985;248(3 Pt 1):E353-362.
18. Kang L, Lantier L, Kennedy A, Bonner JS, Mayes WH, Bracy DP, Bookbinder LH, Hasty AH, Thompson CB, Wasserman DH. Hyaluronan accumulates with high-fat feeding and contributes to insulin resistance. *Diabetes.* 2013;62(6):1888-1896.
19. Kang L, Mayes WH, James FD, Bracy DP, Wasserman DH. Matrix metalloproteinase 9 opposes diet-induced muscle insulin resistance in mice. *Diabetologia.* 2014;57(3):603-613.
20. Matsumoto T, Turesson I, Book M, Gerwins P, Claesson-Welsh L. p38 MAP kinase negatively regulates endothelial cell survival, proliferation, and differentiation in FGF-2-stimulated angiogenesis. *The Journal of cell biology.* 2002;156(1):149-160.
21. McCall-Culbreath KD, Zutter MM. Collagen receptor integrins: rising to the challenge. *Curr Drug Targets.* 2008;9(2):139-149.
22. Williams AS, Kang L, Zheng J, Grueter C, Bracy DP, James FD, Pozzi A, Wasserman DH. Integrin alpha1-null mice exhibit improved fatty liver when fed a high fat diet despite severe hepatic insulin resistance. *J Biol Chem.* 2015;290(10):6546-6557.
23. Wickstrom SA, Lange A, Montanez E, Fassler R. The ILK/PINCH/parvin complex: the kinase is dead, long live the pseudokinase! *The EMBO journal.* 2010;29(2):281-291.
24. McDonald PC, Oloumi A, Mills J, Dobreva I, Maidan M, Gray V, Wederell ED, Bally MB, Foster LJ, Dedhar S. Rictor and integrin-linked kinase interact and regulate Akt phosphorylation and cancer cell survival. *Cancer research.* 2008;68(6):1618-1624.
25. Fukuda T, Guo L, Shi X, Wu C. CH-ILKBP regulates cell survival by facilitating the membrane translocation of protein kinase B/Akt. *The Journal of cell biology.* 2003;160(7):1001-1008.
26. Kimura M, Murakami T, Kizaka-Kondoh S, Itoh M, Yamamoto K, Hojo Y, Takano M, Kario K, Shimada K, Kobayashi E. Functional molecular imaging of ILK-mediated Akt/PKB signaling cascades and the associated role of beta-parvin. *Journal of cell science.* 2010;123(Pt 5):747-755.
27. Solomon TP, Haus JM, Li Y, Kirwan JP. Progressive hyperglycemia across the glucose tolerance continuum in older obese adults is related to skeletal muscle capillarization and nitric oxide bioavailability. *The Journal of clinical endocrinology and metabolism.* 2011;96(5):1377-1384.
28. Kadrmas JL, Smith MA, Clark KA, Pronovost SM, Muster N, Yates JR, 3rd, Beckerle MC. The integrin effector PINCH regulates JNK activity and epithelial migration in concert with Ras suppressor 1. *The Journal of cell biology.* 2004;167(6):1019-1024.
29. Habegger KM, Penque BA, Sealls W, Tackett L, Bell LN, Blue EK, Gallagher PJ, Sturek M, Alloosh MA, Steinberg HO, Considine RV, Elmendorf JS. Fat-induced membrane cholesterol accrual provokes cortical filamentous actin destabilisation and glucose transport dysfunction in skeletal muscle. *Diabetologia.* 2012;55(2):457-467.
30. Hao YC, Yu LP, Li Q, Zhang XW, Zhao YP, He PY, Xu T, Wang XF. Effects of integrin-linked kinase on human corpus cavernosum smooth muscle cell cytoskeletal organisation. *Andrologia.* 2013;45(2):78-85.

31. Gheyara AL, Vallejo-Illarramendi A, Zang K, Mei L, St-Arnaud R, Dedhar S, Reichardt LF. Deletion of integrin-linked kinase from skeletal muscles of mice resembles muscular dystrophy due to alpha 7 beta 1-integrin deficiency. *Am J Pathol.* 2007;171(6):1966-1977.

32. Yau CY, Wheeler JJ, Sutton KL, Hedley DW. Inhibition of integrin-linked kinase by a selective small molecule inhibitor, QLT0254, inhibits the PI3K/PKB/mTOR, Stat3, and FKHR pathways and tumor growth, and enhances gemcitabine-induced apoptosis in human orthotopic primary pancreatic cancer xenografts. *Cancer Res.* 2005;65(4):1497-1504.

33. Kalra J, Warburton C, Fang K, Edwards L, Daynard T, Waterhouse D, Dragowska W, Sutherland BW, Dedhar S, Gelmon K, Bally M. QLT0267, a small molecule inhibitor targeting integrin-linked kinase (ILK), and docetaxel can combine to produce synergistic interactions linked to enhanced cytotoxicity, reductions in P-AKT levels, altered F-actin architecture and improved treatment outcomes in an orthotopic breast cancer model. *Breast cancer research : BCR.* 2009;11(3):R25.

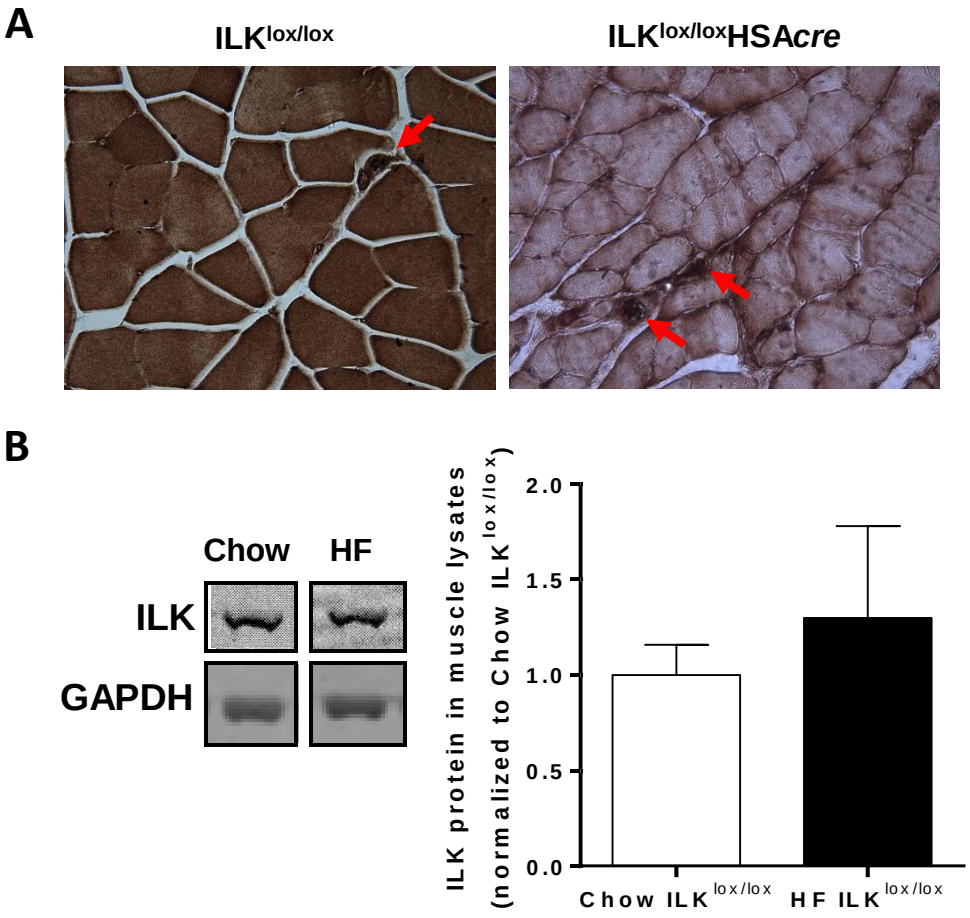
A
ILK lox/lox
ILK lox/lox HSAcre
B
Chow
HF
ILK
GAPDH
ILK protein in muscle lysates
(normalized to Chow ILK lox/lox)
2.0
1.5
1.0
0.5
0.0
Chow ILK lox/lox
HF ILK lox/lox

Figure 1

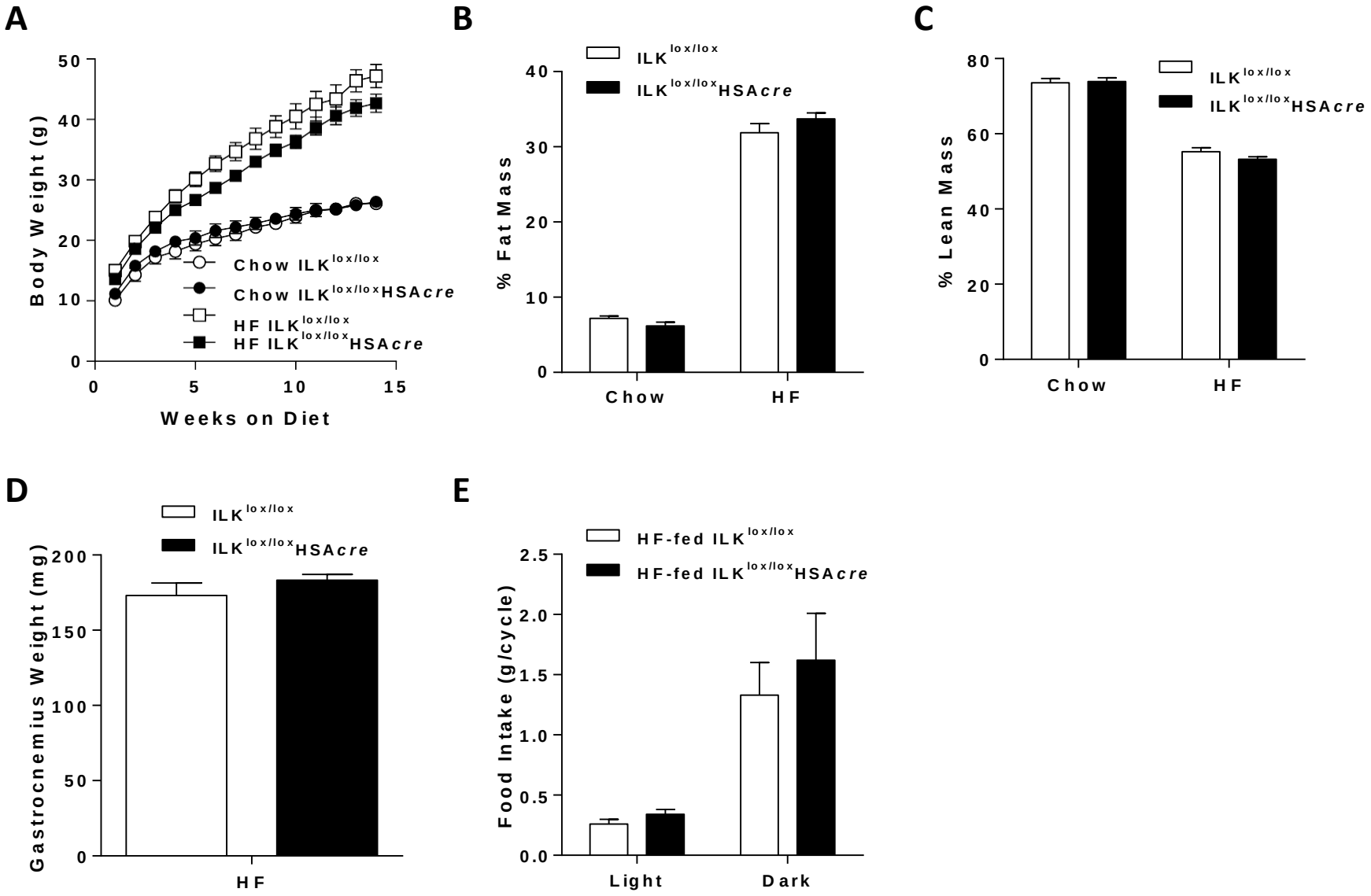
A
Body Weight (g)
Weeks on Diet
Chow ILK lox/lox
Chow ILK lox/lox HSAcre
HF ILK lox/lox
HF ILK lox/lox HSAcre
B
% Fat Mass
ILK lox/lox
ILK lox/lox HSAcre
Chow
HF
C
% Lean Mass
ILK lox/lox
ILK lox/lox HSAcre
Chow
HF
D
Gastrocnemius Weight (mg)
ILK lox/lox
ILK lox/lox HSAcre
HF
E
Food Intake (g/cycle)
HF-fed ILK lox/lox
HF-fed ILK lox/lox HSAcre
Light
Dark

Figure 2

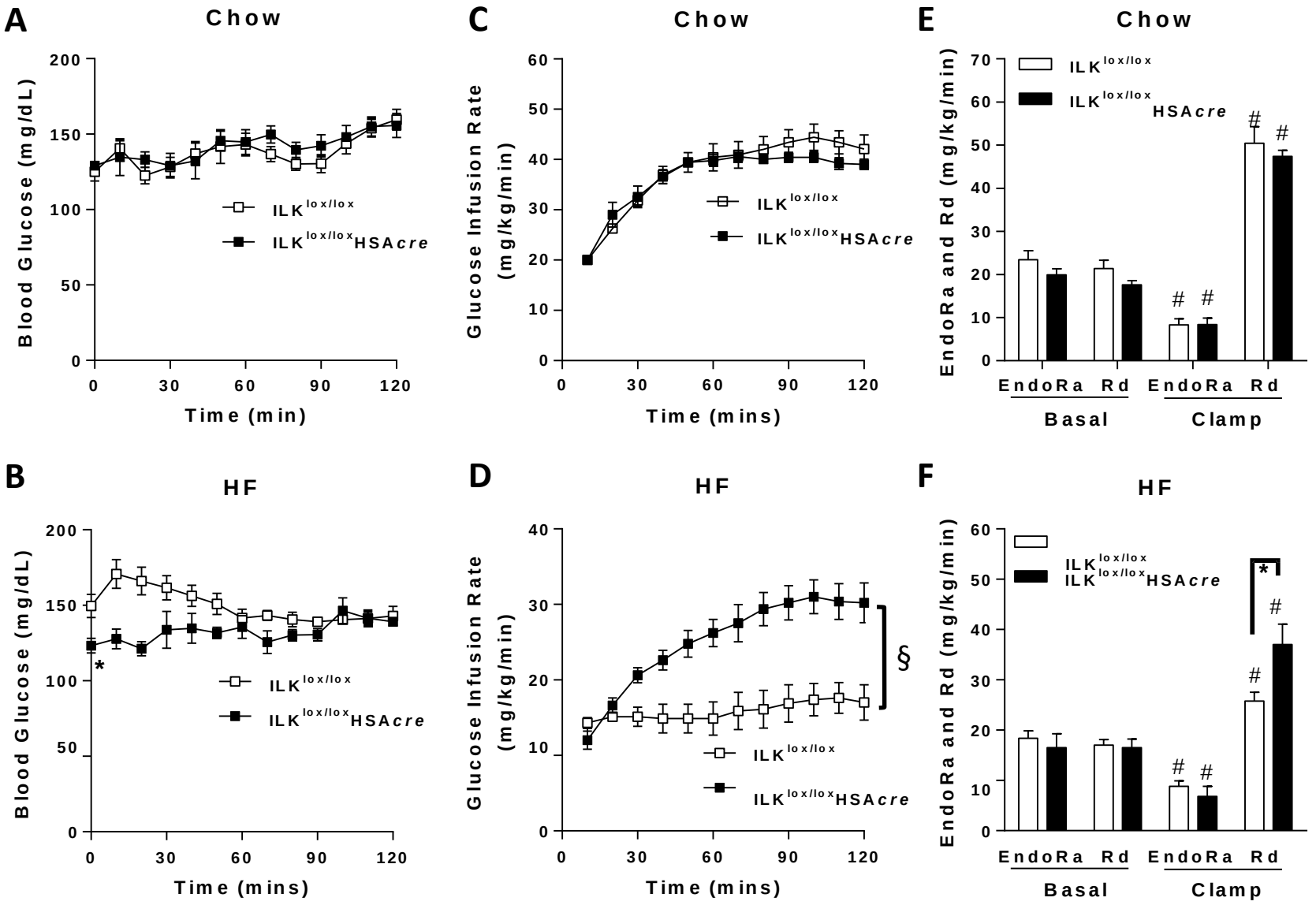
A
Chow
Blood Glucose (mg/dL)
Time (min)
ILK lox/lox
ILK lox/lox HSAcre
B
HF
Blood Glucose (mg/dL)
Time (mins)
*
C
Chow
Glucose Infusion Rate (mg/kg/min)
Time (mins)
D
HF
Glucose Infusion Rate (mg/kg/min)
Time (mins)
§
E
Chow
EndoRa and Rd (mg/kg/min)
EndoRa Rd EndoRa Rd
Basal
Clamp
#
F
HF
EndoRa and Rd (mg/kg/min)
*

Figure 3

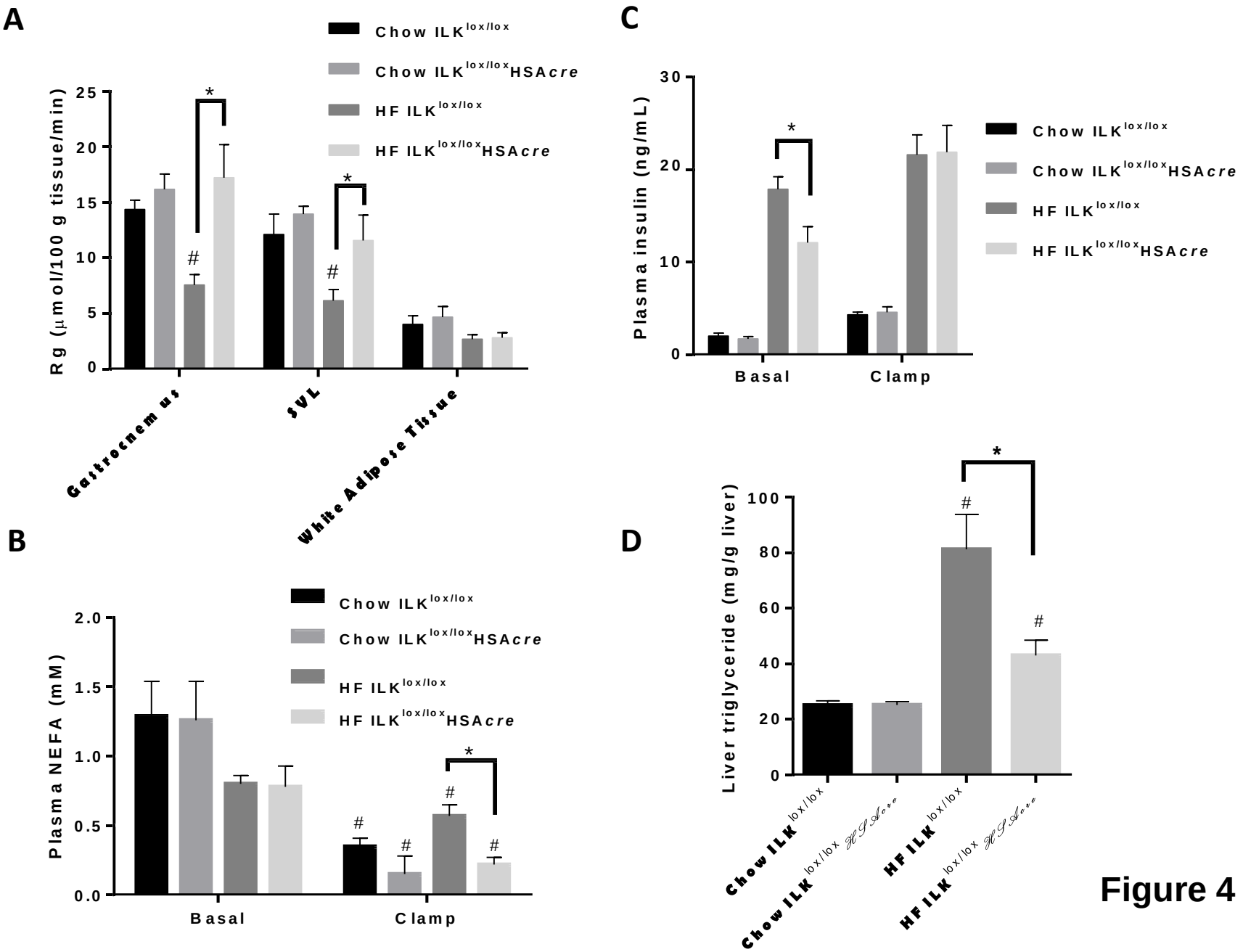
A
Chow ILK lox/lox
Chow ILK lox/lox HSAcre
HF ILK lox/lox
HF ILK lox/lox HSAcre
Rg (µmol/100 g tissue/min)
25
20
15
10
5
0
*
*
#
#
Gastrocnemius
SVL
White Adipose Tissue
C
Plasma insulin (ng/mL)
30
20
10
0
*
Basal
Clamp
Chow ILK lox/lox
Chow ILK lox/lox HSAcre
HF ILK lox/lox
HF ILK lox/lox HSAcre
B
Plasma NEFA (mM)
2.0
1.5
1.0
0.5
0.0
Chow ILK lox/lox
Chow ILK lox/lox HSAcre
HF ILK lox/lox
HF ILK lox/lox HSAcre
*
#
#
#
#
Basal
Clamp
D
Liver triglyceride (mg/g liver)
100
80
60
40
20
0
*
#
#
Chow ILK lox/lox
Chow ILK lox/lox HSAcre
HF ILK lox/lox
HF ILK lox/lox HSAcre

Figure 4

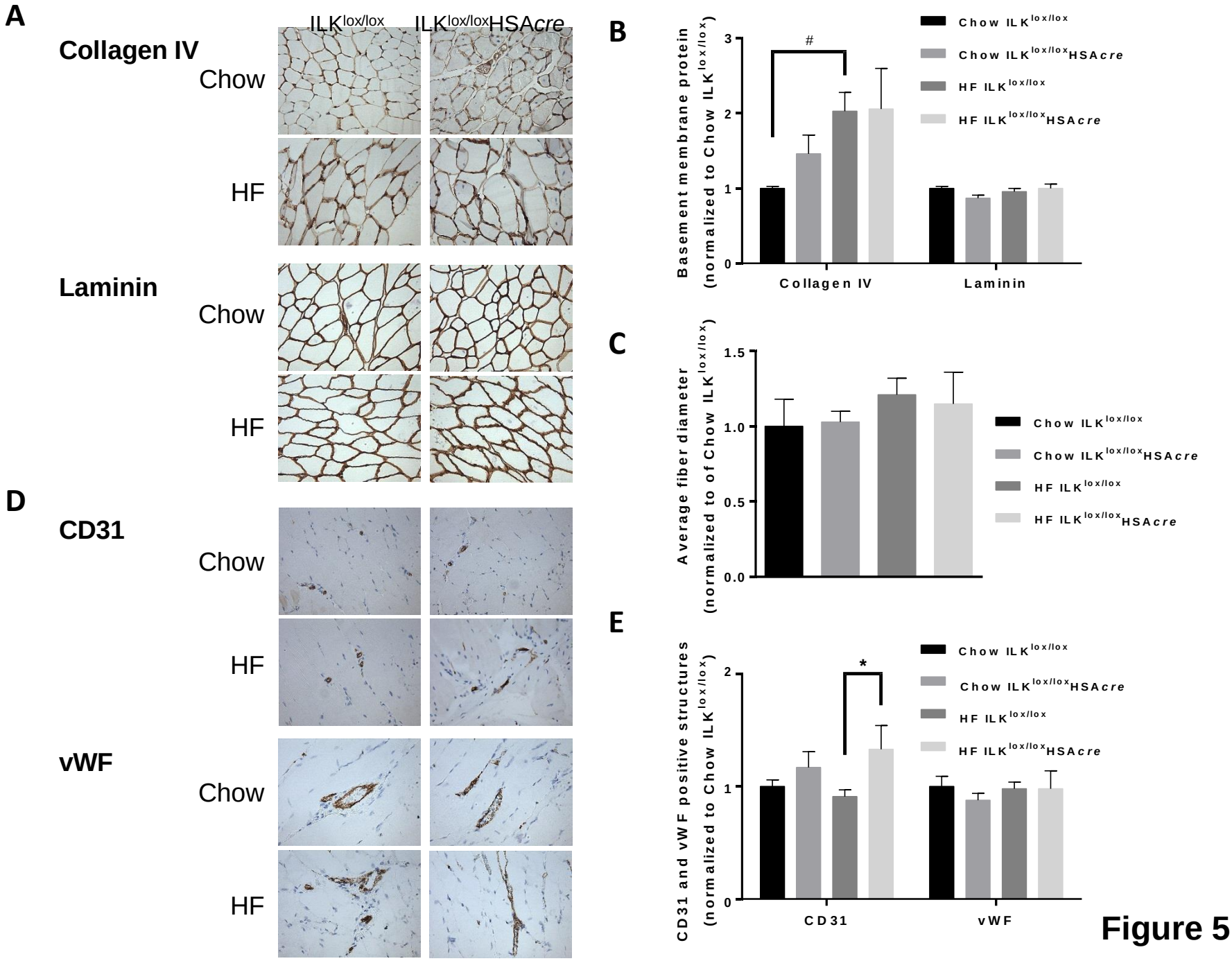
A
ILK lox/lox
ILK lox/lox HSAcre
Collagen IV
Chow
HF
Laminin
Chow
HF
D
CD31
Chow
HF
vWF
Chow
HF
B
Basement membrane protein (normalized to Chow ILK lox/lox)
#
Chow ILK lox/lox
Chow ILK lox/lox HSAcre
HF ILK lox/lox
HF ILK lox/lox HSAcre
Collagen IV
Laminin
C
Average fiber diameter (normalized to of Chow ILK lox/lox)
Chow ILK lox/lox
Chow ILK lox/lox HSAcre
HF ILK lox/lox
HF ILK lox/lox HSAcre
E
CD31 and vWF positive structures (normalized to Chow ILK lox/lox)
*
Chow ILK lox/lox
Chow ILK lox/lox HSAcre
HF ILK lox/lox
HF ILK lox/lox HSAcre
CD31
vWF

Figure 5

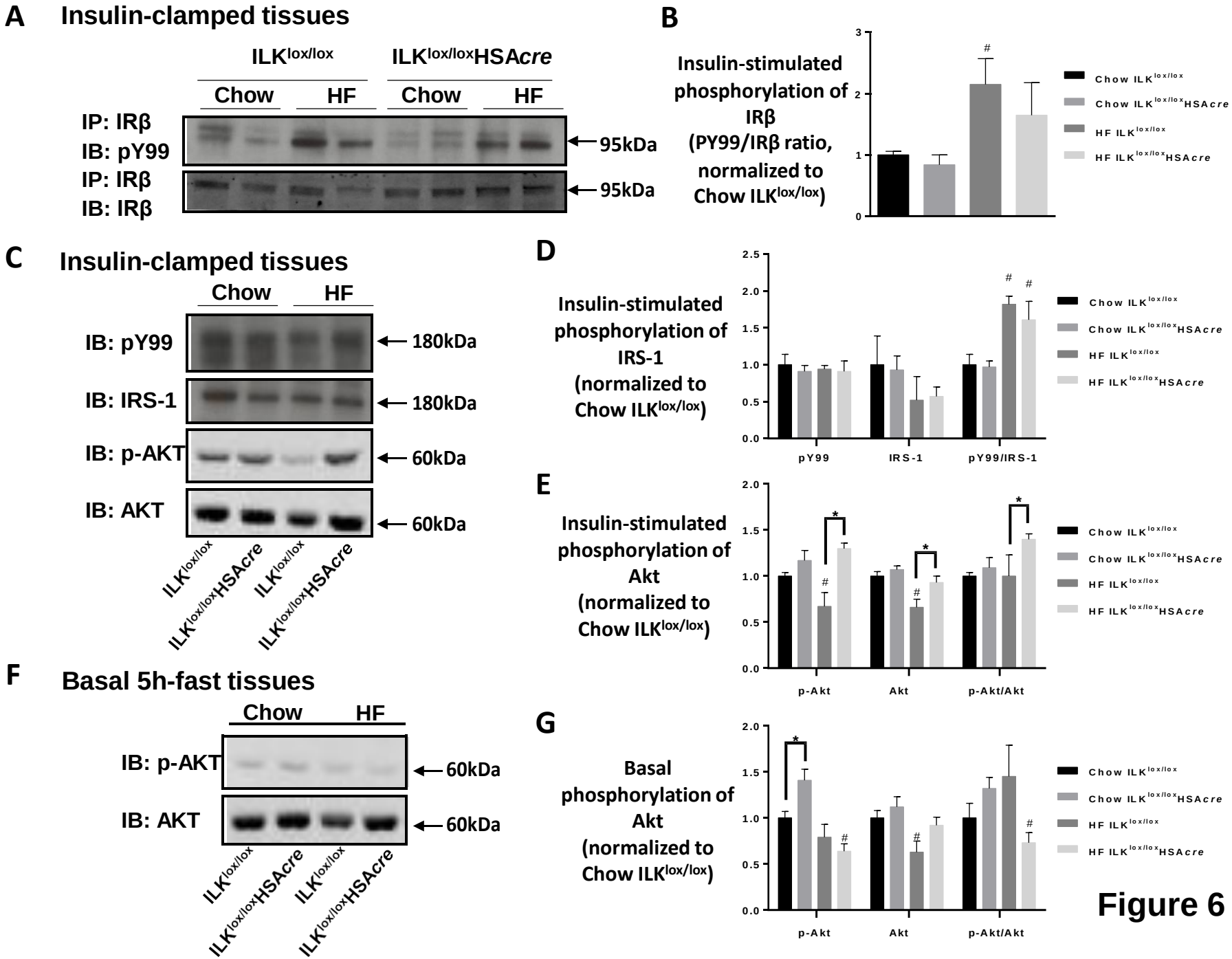
A
Insulin-clamped tissues
ILK lox/lox
ILK lox/lox HSAcre
Chow
HF
Chow
HF
IP: IRβ
IB: pY99
IP: IRβ
IB: IRβ
95kDa
95kDa
B
Insulin-stimulated phosphorylation of IRβ (PY99/IRβ ratio, normalized to Chow ILK lox/lox)
Chow ILK lox/lox
Chow ILK lox/lox HSAcre
HF ILK lox/lox
HF ILK lox/lox HSAcre
C
Insulin-clamped tissues
Chow
HF
IB: pY99
IB: IRS-1
IB: p-AKT
IB: AKT
180kDa
180kDa
60kDa
60kDa
ILK lox/lox
ILK lox/lox HSAcre
ILK lox/lox
ILK lox/lox HSAcre
D
Insulin-stimulated phosphorylation of IRS-1 (normalized to Chow ILK lox/lox)
pY99
IRS-1
pY99/IRS-1
E
Insulin-stimulated phosphorylation of Akt (normalized to Chow ILK lox/lox)
p-Akt
Akt
p-Akt/Akt
F
Basal 5h-fast tissues
Chow
HF
IB: p-AKT
IB: AKT
60kDa
60kDa
ILK lox/lox
ILK lox/lox HSAcre
ILK lox/lox
ILK lox/lox HSAcre
G
Basal phosphorylation of Akt (normalized to Chow ILK lox/lox)
p-Akt
Akt
p-Akt/Akt

Figure 6

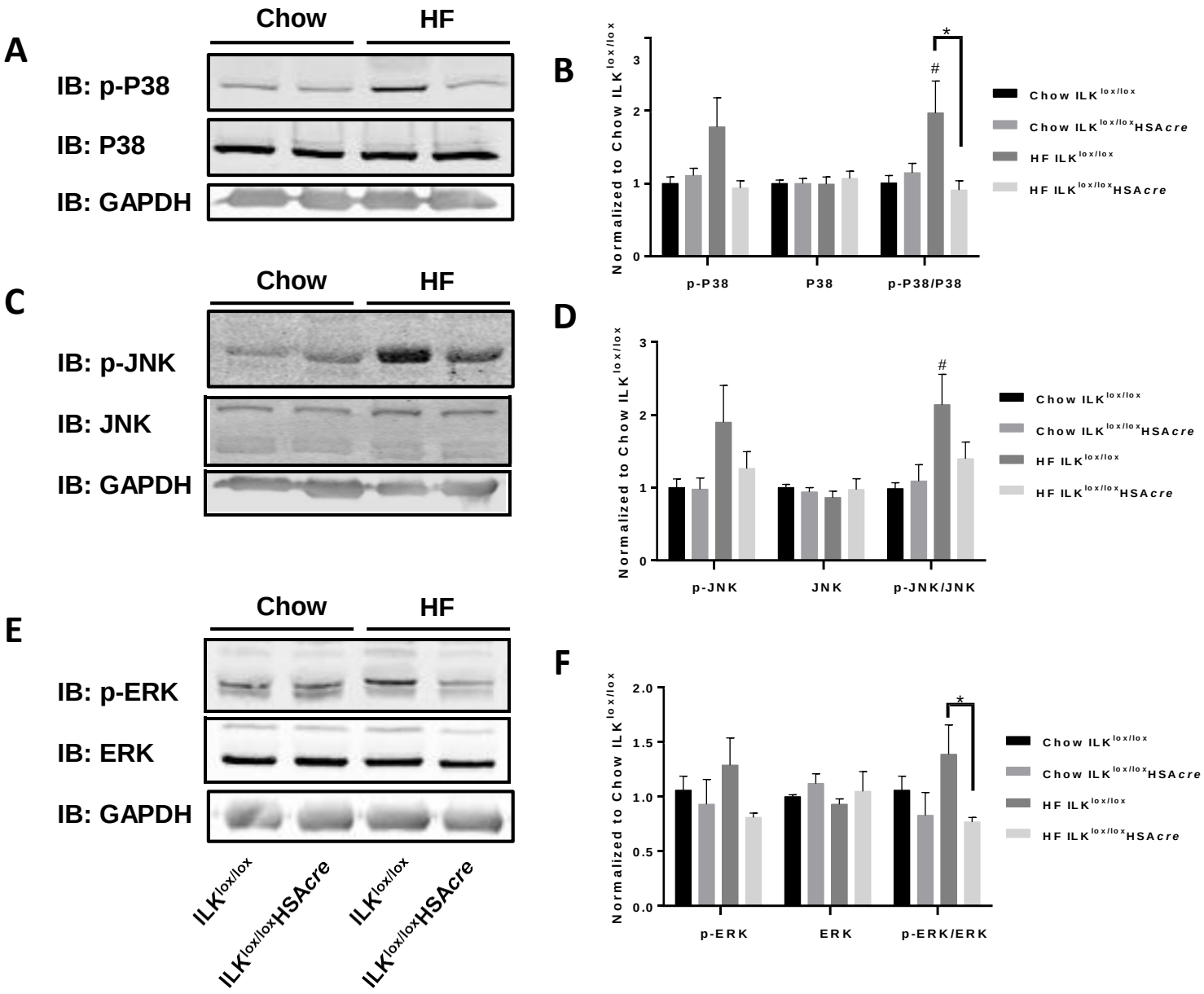
A
Chow
HF
IB: p-P38
IB: P38
IB: GAPDH
B
Normalized to Chow ILK lox/lox
p-P38
P38
p-P38/P38
Chow ILK lox/lox
Chow ILK lox/lox HSAcre
HF ILK lox/lox
HF ILK lox/lox HSAcre
C
IB: p-JNK
IB: JNK
IB: GAPDH
D
p-JNK
JNK
p-JNK/JNK
E
IB: p-ERK
IB: ERK
IB: GAPDH
F
p-ERK
ERK
p-ERK/ERK
ILK lox/lox
ILK lox/lox HSAcre
ILK lox/lox
ILK lox/lox HSAcre

Figure 7

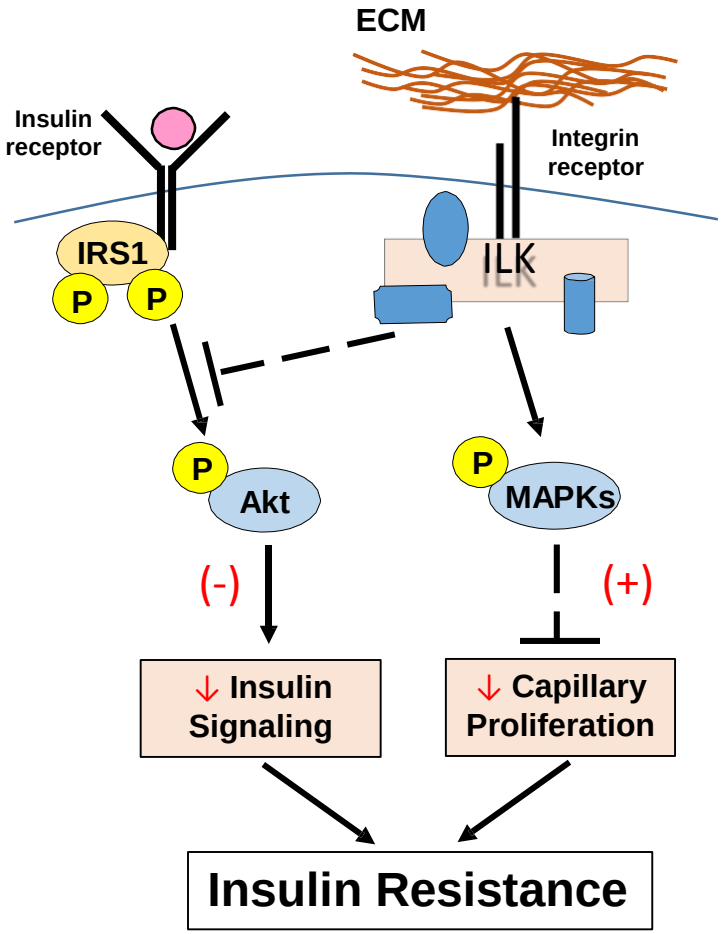
ECM
Insulin receptor
Integrin receptor
IRS1
P
P
ILK
P
Akt
P
MAPKs
(-)
(+)
↓ Insulin Signaling
↓ Capillary Proliferation
Insulin Resistance

Figure 8

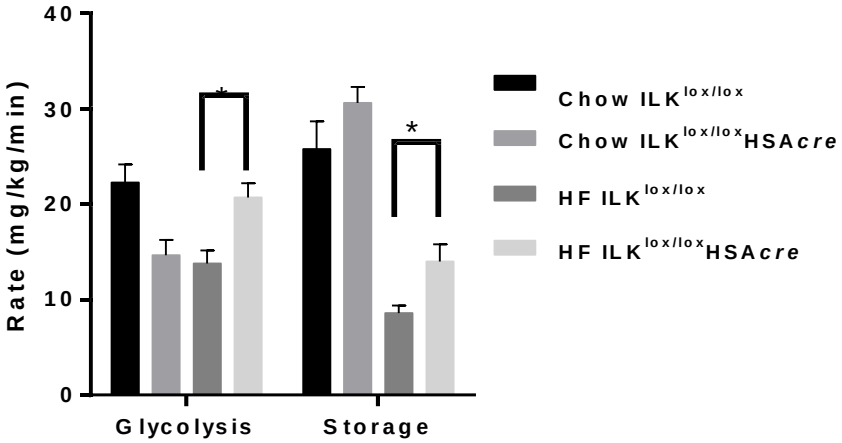

Figure S1 Increased clamp Rd in HF-fed ILK$^{lox/lox}$HSA*cre* mice was due to both increased glycolytic and storage rates. Glycolysis was calculated by the rate of ^{3}H-H_2O accumulation in plasma during the ICv clamp and glucose storage rate (mainly glycogen) was calculated by subtracting the glycolytic rate from total clamp Ra/Rd (n=5-9). All data are represented as mean ± SEM. *p<0.05. HF, high fat.

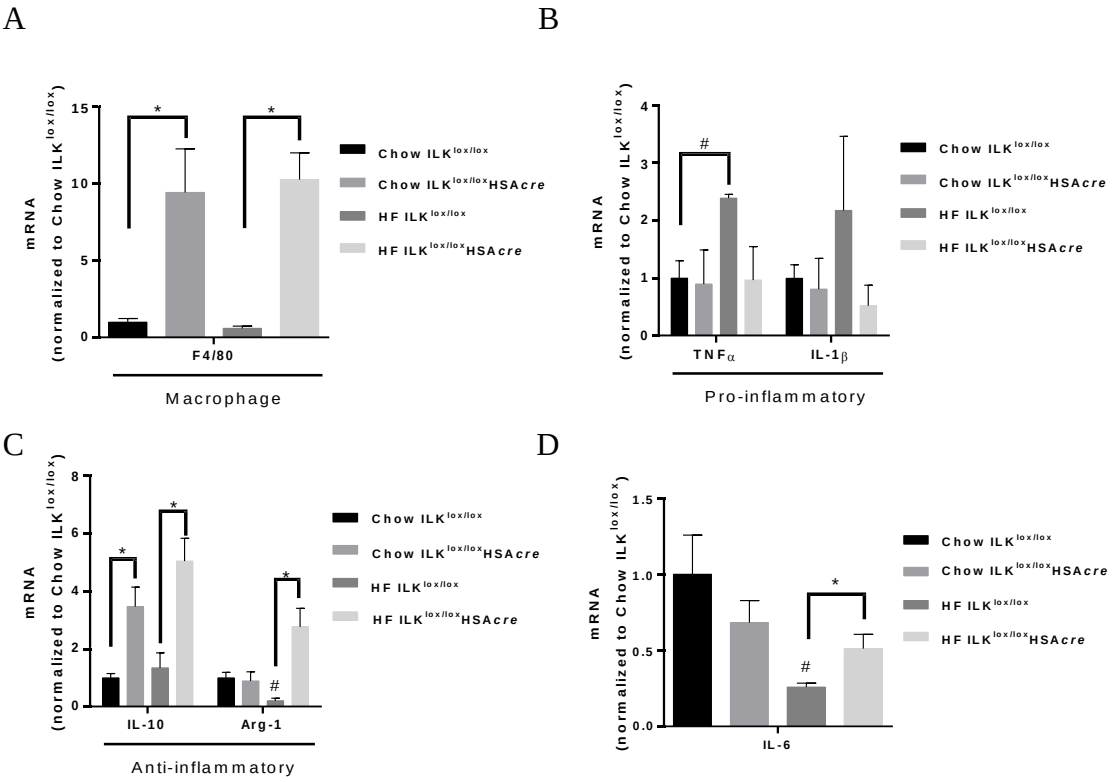

Figure S2 Muscle-specific deletion of ILK caused changes in the status of adipose inflammation. This was possibly due to increased IL-6 secreted from muscle of HF-fed ILK$^{lox/lox}$HSA*cre* mice compared to HF-fed ILK$^{lox/lox}$ mice. Gene expression in gonadal adipose tissue (A-C) and gastrocnemius muscle (D) was determined by real-time PCR. RNA was isolated from 50 mg of tissues using the Tri-reagent. cDNA was synthesized using Superscript II (Invitrogen). Real-time PCR analysis was performed using Taqman gene expression assays. The final relative concentration was calculated by $2^{(50-Ct)}$ and was normalized to GAPDH. (A) Gene expression of total macrophage marker F4/80 in adipose tissue (n=3-5). (B) Gene expression of the pro-inflammatory markers TNFα and IL-1β in adipose tissue (n=3-5). (C) Gene expression of the anti-inflammatory markers IL-10 and Arg-1 in adipose tissue (n=3-5). (D) Gene expression of IL-6 in muscle (n=4-6). All data are represented as mean ± SEM. $^{\#}p<0.05$ compared with chow-fed mice with the same genotype. $*p<0.05$ compared with ILK$^{lox/lox}$ with the same diet. HF, high fat.